Plasma Sources Sci. Technol. **20** (2011) 055001 (9pp) doi:10.1088/0963-0252/20/5/055001

Control of ion energy distributions using a pulsed plasma with synchronous bias on a boundary electrode

Hyungjoo Shin, Weiye Zhu, Lin Xu[1], Vincent M Donnelly and Demetre J Economou

Plasma Processing Laboratory, Department of Chemical and Biomolecular Engineering, University of Houston, Houston, TX 77204-4004, USA

E-mail: vmdonnelly@uh.edu and economou@uh.edu

Received 23 November 2010, in final form 18 April 2011
Published 11 August 2011
Online at stacks.iop.org/PSST/20/055001

Abstract
Ion energy distributions (IEDs) on a grounded substrate in a Faraday-shielded argon inductively coupled plasma were measured with a retarding field energy analyzer. A Langmuir probe was also used to measure space- and time-resolved plasma parameters. IEDs and plasma parameters were studied with continuous or pulsed positive dc bias voltage on a 'boundary electrode' in contact with the plasma. For continuous wave plasmas without applied bias, the IED exhibited a single broad peak at the plasma potential. Applying a continuous positive dc bias on the boundary electrode shifted the peak of the IED to higher energy. Application of a synchronous dc bias on the boundary electrode during the afterglow of a pulsed plasma resulted in a double-peaked IED. The mean energies of the two peaks, as well as the peak separation, were controlled by adjusting the applied dc bias and the discharge pressure. The full width at half maximum (FWHM) of the peak corresponding to the synchronous dc bias diminished with decreasing electron temperature. The FWHM was controlled by varying the time window in the afterglow during which dc bias was applied.

(Some figures in this article are in colour only in the electronic version)

1. Introduction

Energetic ion bombardment of the substrate is critical for both plasma etching and deposition [1, 2]. In plasma etching, the ion energy must be high enough to promote anisotropic etching, but not so high as to cause sputtering, substrate damage or loss of selectivity with respect to the mask or the underlying substrate. To achieve the higher selectivity and line width control that will be required for future devices, not only the mean ion energy but also the ion energy distribution (IED) must be controlled. For example, in etching of SiO_2 in fluorocarbon plasmas, Wang and Wendt [3] have shown that tailored bias waveforms [4, 5] produce narrow IEDs that allow the energy of ions bombarding the substrate to be above the threshold for SiO_2 ion-stimulated etching, but below the threshold for Si etching, thereby enabling extremely high selectivity of SiO_2 over Si.

[1] Currently with Lam Research, Fremont, CA, USA.

If current trends continue, plasma etching will soon be called upon for applications in which monolayer control is required. Consequently, some form of atomic layer etching will be necessary. Early efforts to achieve atomic layer, self-limited etching have shown the importance of a nearly monoenergetic ion flux with a tightly controlled width of the IED, such that the ion energies are between the thresholds for chemical sputtering and physical sputtering of the substrate [6, 7]. Monoenergetic ions are also useful for other advanced patterning methods, including neutral beam etching [8, 9] and nanopantography [10, 11]. In the latter method, a monoenergetic ion beam is required to achieve optimum focusing of the beam, and consequently minimize the size of nano-patterns that are etched or deposited on the substrate.

The IED may be controlled by applying a bias on the substrate or on an electrode in contact with the plasma. The application of radio frequency (rf) bias normally results in a bimodal IED [12–18]. When $\tau_i \ll \tau$ (where τ is the period of

 © 2011 IOP Publishing Ltd Printed in the UK & the USA

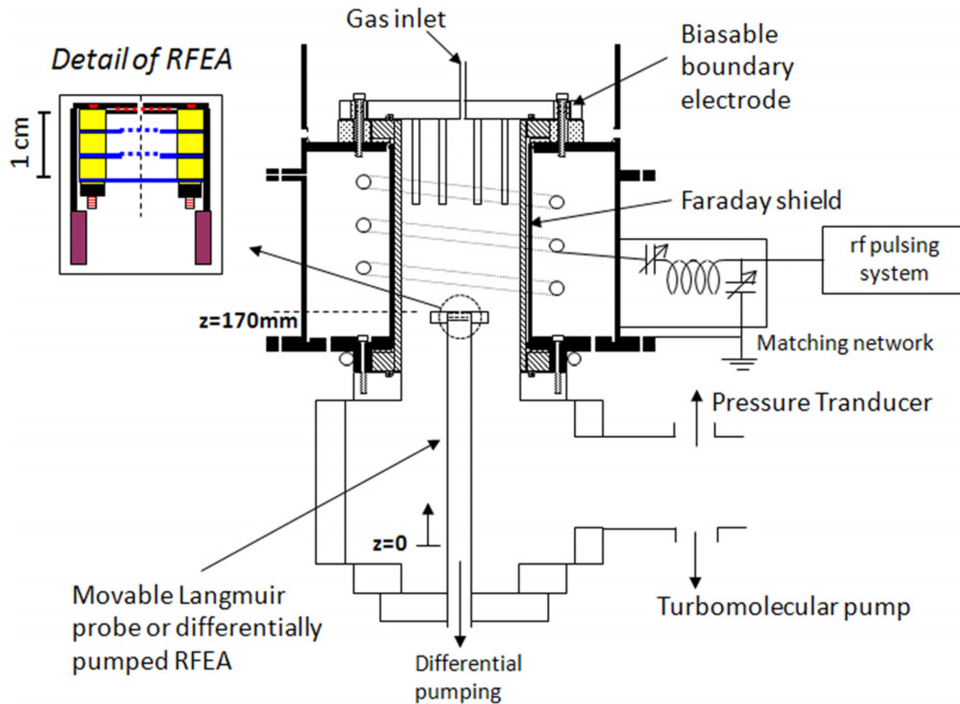

Figure 1. Schematic of the experimental system. The retarding field energy analyzer (RFEA) could be replaced by a movable Langmuir probe (LP) to perform spatially resolved measurements. The inset shows details of the RFEA.

the applied bias and τ_i is the ion transit time through the sheath), ions respond to the instantaneous sheath voltage, and the IED is rather broad. As τ_i/τ increases, the width of the distribution decreases and, for very high τ_i/τ, the IED becomes single peaked. However, for very high frequencies (very small τ), the wavelength of the applied field may become comparable to the substrate dimension, resulting in undesirable effects, such as non-uniform voltage distribution on the substrate electrode [20].

Other investigators have controlled the IED by applying a bias on a separate electrode in contact with the plasma. For example, Smith and Overzet [21] and Coburn and Kay [22] applied bias to a metal electrode, thereby shifting the plasma potential (V_P) and modifying the IED on the substrate. A similar approach was followed by Panda *et al* [8], in controlling the energy of fast neutrals emanating from a neutral beam source. Application of a bias on a 'boundary electrode' raised the plasma potential and expelled positive ions out of the plasma, through a metal grid with high aspect ratio holes. The ions were naturalized on the grid by undergoing grazing angle collisions with the walls, thereby yielding a fast neutral beam. Xu *et al* [23] obtained nearly monoenergetic IEDs by applying a dc bias on a boundary electrode in a pulsed capacitively coupled plasma. By applying the bias synchronously in the afterglow they were able to minimize the width of the distribution.

In this study, the IED was controlled by applying a synchronous positive dc bias to a boundary electrode during the afterglow of a Faraday-shielded inductively coupled pulsed plasma. In contrast to Xu *et al* [23], this work focuses on relatively low ion energies. Space- and time-resolved Langmuir probe (LP) measurements were used to monitor important plasma parameters to help explain the dependence of the IEDs on reactor operating conditions.

2. Experimental apparatus

2.1. Plasma source

Figure 1 shows a schematic of the experimental apparatus used in this study. The inductively coupled plasma (ICP) was ignited by a 3-turn spiral coil in a 17.8 cm long, 8.6 cm inside diameter alumina tube. A copper Faraday shield prevented capacitive coupling between the coil and the plasma. The discharge tube was connected to a cubical stainless steel (SS) chamber through an adaptor flange. A water channel in that flange served to cool the Faraday shield and prevent overheating of the discharge tube. The system was pumped by a 300 $\mathrm{l\,s^{-1}}$ turbopump backed by a dry pump. Pressure was measured by an MKS 629 (0.1 Torr full scale) capacitance manometer mounted downstream of the plasma. Little change (<5% increase) was observed in this pressure when the plasma was ignited. A calibration experiment, without plasma, showed that the pressure at the discharge region was about 30–40% higher than that measured at the position of the pressure gauge. Pressures reported below are all calibrated values and refer to the plasma region.

An SS electrode (henceforth called the 'boundary electrode') comprised the top of the plasma source (figure 1). The boundary electrode had three coaxial cylindrical SS rings welded to the electrode to increase the total surface area to about 300 $\mathrm{cm^2}$ and minimize sputtered metal from coating the chamber. The large surface area was found to be necessary during LP measurements when the probe was biased close to V_P. A large grounded surface was then required to supply

an adequate electron current, preventing an artificial increase in V_P. (A reference electrode on the LP corrects for such a shift in V_P, up to all but the highest plasma densities investigated here.) Argon gas (high purity, 99.999%) was fed into the discharge tube through a 1 mm diameter hole at the center of the boundary electrode.

Plasma power at 13.56 MHz was supplied using a function generator (Hewlett Packard model 3325A) feeding a power amplifier (ENI model A-500). The output of the amplifier was connected to the coil via an L-type matching network. Forward and reflected power was monitored by in-line Bird meters placed before the matching network. For a typical continuous wave (cw) 300 W Ar plasma at 14 mTorr, the reflected power was 1–2 W. The actual power dissipated in the plasma is somewhat lower than the net power delivered to the matching box due to power losses. For pulsed-plasma operation, the rf pulse was amplitude-modulated by another function generator (BNC model 645). Waveforms were monitored using a four-channel oscilloscope (Tektronix model TDS 2024B). Base case conditions for pulsed-plasma experiments were 120 W time-average forward power, 8 W reflected power, 10 kHz power modulation frequency, 20% duty cycle, 14 mTorr pressure and 40 sccm argon gas flow rate. The applied modulation frequency and duty cycle resulted in 20 μs plasma ON time and 80 μs plasma OFF (afterglow) time, during the 100 μs period of a pulse.

2.2. Plasma diagnostics

2.2.1. Langmuir probe. An LP (Scientific Systems Smart Probe) was used to measure ion and electron densities (n_i and n_e), plasma potentials (V_P), floating potentials and electron energy probability functions (EEPF) [24, 25]. The cylindrical tungsten probe tip had a diameter of 0.19 mm and an exposed length of 4.0 mm. A compensation electrode and rf chokes minimized distortion of the I–V characteristic due to oscillations of the plasma potential. This was not an issue in the present system where, due to the Faraday shield, peak-to-peak plasma potential oscillations were only 1–2 V. The probe was movable along the discharge tube axis to obtain spatially resolved measurements. Fast data acquisition electronics enabled averaging of 100 s of I–V characteristics (at a given location and for given plasma conditions) to reduce noise. The current–voltage (I–V) characteristics were interpreted using the software supplied by the manufacturer. This analysis relies on Laframboise's orbital motion-limited (OML) theory for a collisionless sheath. When the Debye length does not exceed the cylindrical probe radius (r_p), it has been shown [26] that collisions can be ignored, and the OML theory applies, when

$$\lambda_i/r_p > (e(V_P - V)/kT_i)^{1/2}, \quad (1)$$

where λ_i is the ion–neutral mean free path, V is the voltage on the probe and T_i is the ion temperature. For the probe used in this study, $r_p = 0.095$ mm. At 10 mTorr Ar, $\lambda_i = 1.5$ mm, hence the right-hand side of equation (1) must be <16 to ignore collisions. Assuming $T_i \approx 0.1$ eV, errors will be made when V_P–V exceeds 25 V. V_P is typically 15 V, hence the ion current will be affected by collisions when the voltage on the probe is more negative than −10 V. Since positive ion densities were extracted from the ion saturation regime of the I–V characteristic by applying voltages in the range ∼0 to −50 V, the derived positive ion densities can be affected at pressures of ∼10 mTorr and above. The measured ion current can be enhanced or suppressed due to collisions [27]. It appears in the current study that an enhancement in ion current would be expected, hence the somewhat higher ion densities relative to electron densities measured at 14 and 28 mTorr (figure 2) could be due to collisions.

The probe was also operated in an internally applicable 'boxcar' mode to measure time-resolved plasma characteristics during pulsed-plasma operation [28, 29].

2.2.2. Retarding field energy analyzer. A retarding field energy analyzer (RFEA) was constructed to measure the energy distributions of ions passing through a grid on the grounded stage. The RFEA was made of a stack of three nickel grids and an SS current collector plate (see the inset in figure 1), spaced 3 mm apart. The top grid (50% open with square holes 18 μm on a side) was attached to a grounded SS plate with a 0.3 mm pinhole in contact with the plasma. This grid prevented the plasma sheath from molding over the pinhole [30]. The middle and bottom grids were each 85% open with square holes 293 μm on a side. The middle grid was biased with −30 V to repel electrons from the plasma, while the bottom grid was biased with a saw-tooth ramp voltage and served as an energy discriminator to measure the IED. A current amplifier (Keithley model 427) was used to measure the ion current on the collector plate. A 20 Hz ramp voltage was applied to the discriminator grid using a pulse generator and a power amplifier (Avtech AVR-3-PS-P-UHF and AV-112AH-PS). The experiment was controlled through a LabVIEW (National Instruments) program. Noise was reduced by averaging 5000 I–V characteristics resulting in 'smooth' IEDs. The RFEA was differentially pumped by a 210 l s^{-1} turbopump to minimize ion–neutral collisions in the analyzer. The pressure in the analyzer was estimated to be two orders of magnitude lower than the pressure in the discharge tube, resulting in collisionless ion flow. The energy resolution of the RFEA was estimated using the formulae of Sakai and Katsumata [31] to be $\sim\Delta E/E = 2\%$.

3. Results and discussion

3.1. Continuous wave plasmas

Figure 2 shows ion and electron densities as a function of vertical position along the discharge tube axis, measured by the LP, for different pressures. Charge density reaches a maximum around the middle of the coil and increases with pressure. A maximum ion density of about 1.5×10^{12} cm^{-3} is reached for a pressure of 50 mTorr. The electron and ion density are nearly equal for pressures of 3, 7, and 14 mTorr. For 28 mTorr, and especially near the center at 50 mTorr, the electron density was lower than the corresponding ion density. This was attributed to the fact that as the probe was biased near V_P, a large electron

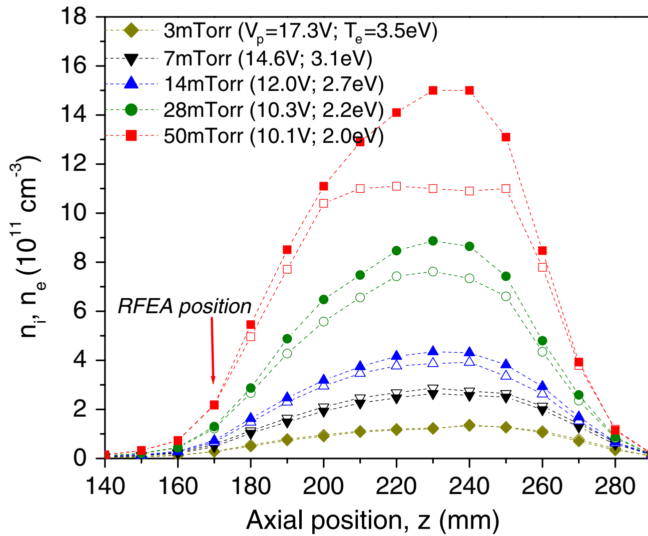

Figure 2. Ion (solid symbols) and electron (open symbols) density as a function of position and pressure measured by the LP for cw plasmas at 300 W and 40 sccm. When in the place of the LP, the RFEA was positioned at $z = 170$ mm as shown by the arrow. The plasma potential and the electron temperature measured by the LP at $z = 170$ mm are shown in parentheses next to the corresponding pressure.

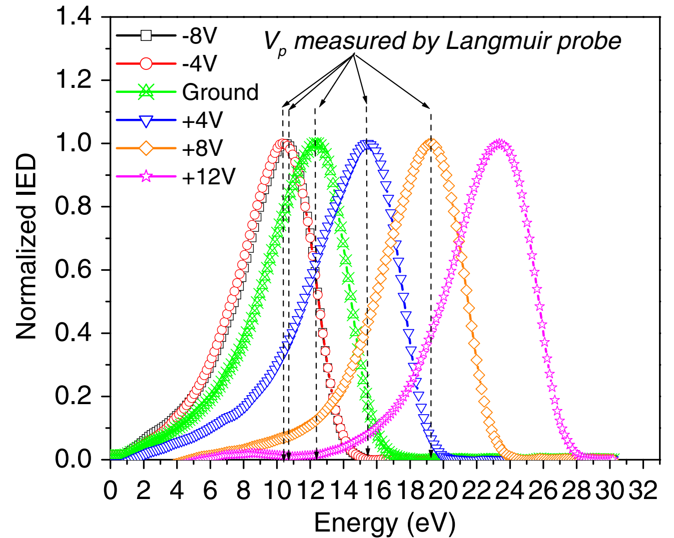

Figure 3. Normalized IEDs measured in cw plasmas (300 W, 14 mTorr, 40 sccm), for different dc bias voltages applied continuously to the boundary electrode. Plasma potentials (V_P) measured at the same location by a LP are shown by vertical dashed lines.

current was drawn out of the plasma. Apparently, the grounded surface of the boundary electrode in contact with the plasma was not large enough to compensate for the electron loss at these high densities. (The LP has a reference electrode that senses this imposed shift in V_P and corrects for it, but only up to the point that the maximum positive voltage on the probe is reached before the correct V_P is observed.)

V_P and T_e measured by the LP at $z = 170$ mm are shown in parentheses next to the corresponding pressure. With the LP removed, the RFEA was positioned at $z = 170$ mm. IEDs measured without any applied bias, for cw plasmas at 300 W power and pressures of 7–50 mTorr, were single peaked at energies nearly equal to V_P, as measured with the LP.

3.1.1. Effect of continuous dc bias on the boundary electrode. Figure 3 shows IEDs for 14 mTorr, 300 W cw Ar plasmas for different values of dc bias, applied *continuously* to the boundary electrode. The values of V_P measured by the LP at the location of the RFEA for each dc bias voltage are shown in figure 3 by a vertical dashed line. The measured V_P values are in excellent agreement with the peak energies of the IED. For positive values of the dc bias, V_P is raised, shifting the IED to higher energies. For negative dc bias, there is an initial small drop in V_P, but it saturates as the applied bias becomes more negative. When compared with measurements without dc bias, the peak of the IED shifts by 3 eV, 7 eV and 11 eV for applied dc bias of 4 eV, 8 eV and 12 V, respectively. The 1 V difference between the applied bias and the peak ion energy is probably due to a slight gradient of V_P. When a negative dc bias is applied, the shift in the peak ion energy saturates at 4 V *lower* than without bias. The shift in V_P with the application of a dc bias on the boundary electrode is readily understood [8, 21, 22]. A positive bias drains electrons from the plasma raising V_P so that all but the highest energy electrons remain confined in the plasma. With the application of a small negative bias (less than a few T_e) V_P becomes less positive as electron current to the boundary electrode is partially cut off. Larger negative bias on the boundary electrode cuts off all electron current but causes negligible change in the ion current, hardly affecting V_P, assuming there is no perturbation of the plasma density or T_e.

3.2. Pulsed plasmas

To obtain nearly monoenergetic ion bombardment it is necessary to reduce the energy spread of ions entering the sheath, as well as maintain a constant sheath potential. Since rf oscillations of the plasma potential are eliminated by the Faraday shield, the spread in the energy of ions entering the sheath scales with T_e [32, 33]. Hence, lowering T_e should reduce the energy spread. T_e can be lowered by modulating the plasma power (pulsed plasma). When a dc bias is applied to the boundary electrode under these conditions, ions can be accelerated to a desired energy with a narrow energy spread.

Figure 4 shows time-resolved LP measurements of electron temperature for different pressures. For a given pressure, T_e increases rapidly after the plasma is turned ON, overshoots and then reaches a steady-state value. The steady-state T_e decreases with increasing pressure, as expected. After the plasma is turned OFF, T_e decreases at a progressively slower rate longer into the afterglow. In addition, T_e decays faster at lower pressure. In Ar plasmas, diffusion to the walls is the dominant cooling mechanism during the afterglow for electrons with energies below the lowest excited state (the $^3P_2$ metastable state at 11.55 eV) [34, 35]. Lower pressure results in faster diffusion rates, and therefore a faster decay of T_e in the afterglow.

3.2.1. Continuous dc bias on the boundary electrode. Figure 5 shows IEDs under pulsed-plasma conditions, when

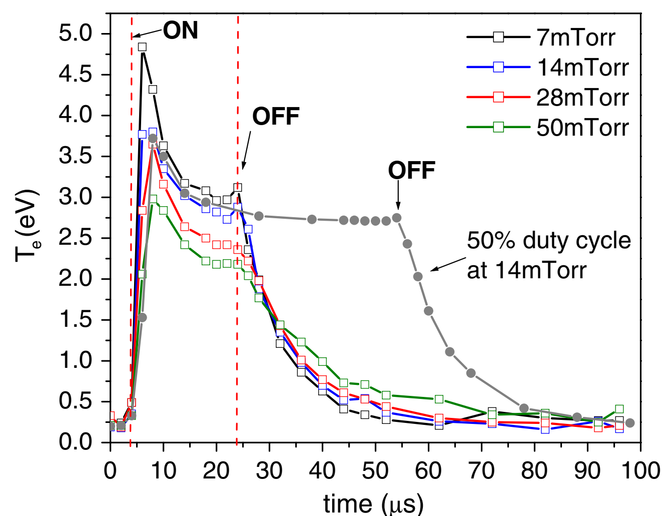

Figure 4. Time-resolved electron temperatures (T_e) measured by the LP in pulsed Ar plasmas generated at 10 kHz power modulation with 20% duty cycle at different pressures, with 120 W time-average power and 40 sccm gas flow. Solid dots are data for a duty cycle of 50% at 14 mTorr.

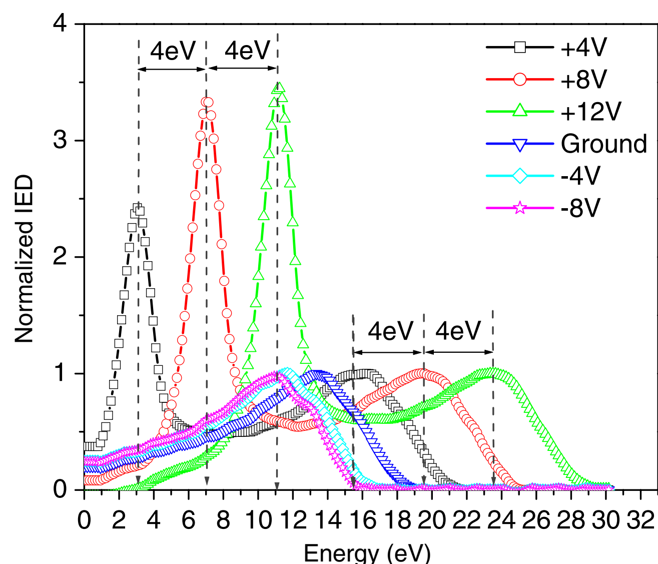

Figure 5. Normalized IEDs under pulsed-plasma conditions with a dc bias applied continuously on the boundary electrode. Other conditions: 120 W average forward power (8 W reflected), 10 kHz plasma power modulation frequency at 20% of duty cycle, 14 mTorr, 40 sccm.

a dc bias was continuously applied to the boundary electrode. For each value of the dc bias, the IED has two peaks. The broader peaks at higher energy correspond to ions bombarding the substrate when the plasma is ON. The shape and energy of these peaks are nearly identical to those observed in the cw plasma (figure 3). The sharper peaks at lower energy correspond to ions bombarding the substrate during the afterglow. The mean energy of these peaks corresponds to the applied dc bias. In the afterglow, V_P reaches a very low value in the absence of dc bias. When a positive dc bias is applied, the plasma potential is approximately equal to the dc bias [11, 36]. The width of the IED is much smaller in the afterglow because of the rapid quenching of electron energy

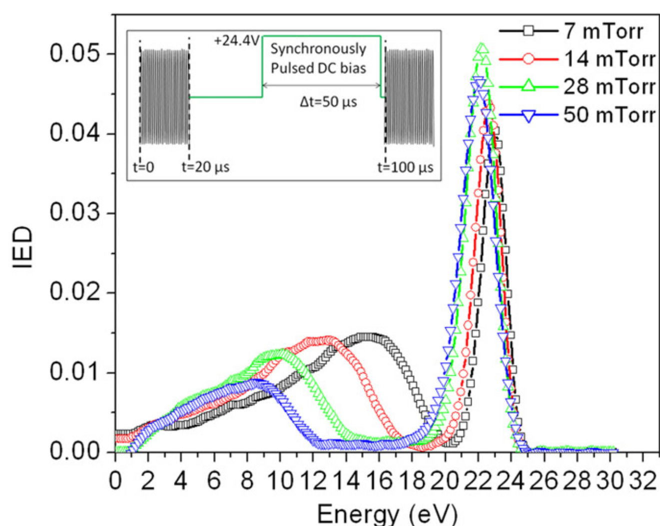

Figure 6. IEDs for different pressures under pulsed-plasma conditions with a synchronous +24.4 V bias applied on the boundary electrode in the afterglow, over the time window, $\Delta t_b = 45$–$95\ \mu$s. Other conditions: 10 kHz plasma power modulation frequency at 20% duty cycle, 120 W average power and 40 sccm gas flow. The inset is a timing diagram showing the applied bias in relation to the plasma on and off times.

(i.e. lower T_e). Similar results were reported by Xu *et al* who obtained a nearly monoenergetic IED by applying a dc bias in the afterglow of a pulsed capacitively coupled plasma [11].

3.2.2. Synchronous (pulsed) dc bias on the boundary electrode. While the above approach creates a narrow and tunable IED, it also leaves a broad and not well-controlled population of ions that enter the sheath during the plasma-ON portion of the cycle. One can reduce the energy of these ions below the threshold for most ion-assisted surface reactions by turning off the dc bias voltage during the plasma-ON periods. In the rest of the paper, results are reported from such pulsed-plasma operation with a synchronous (pulsed) positive dc bias applied to the boundary electrode at specified times during the afterglow.

3.2.2.1. Effect of pressure. The IEDs measured by applying a *synchronous* bias of +24.4 VDC in the afterglow, during the time window $\Delta t_b = 45$–$95\ \mu$s, for different values of pressure are shown in figure 6. The inset is a timing diagram showing the applied bias in relation to the plasma on and off times. The sharp peaks at ∼22–23 V correspond to the dc bias, while the broader peaks at lower energy arise from the plasma ON portion of the cycle. The broader peaks shift to lower energy as pressure increases, due to a concomitant decrease in T_e (in parentheses in figure 2) and hence V_P.

The most important aspect of the two-peaked IEDs shown in figure 6 is that the spacing between a broad peak and the corresponding sharp peak can be varied by varying the dc bias and reactor pressure. Such control is critical for achieving very high selectivity of etching a film relative to the underlying substrate. The pressure can be chosen so that the low energy peak produces no etching. The dc bias can be chosen such that the high energy peak lies between the thresholds of etching the film and etching the substrate, assuming there is sufficient

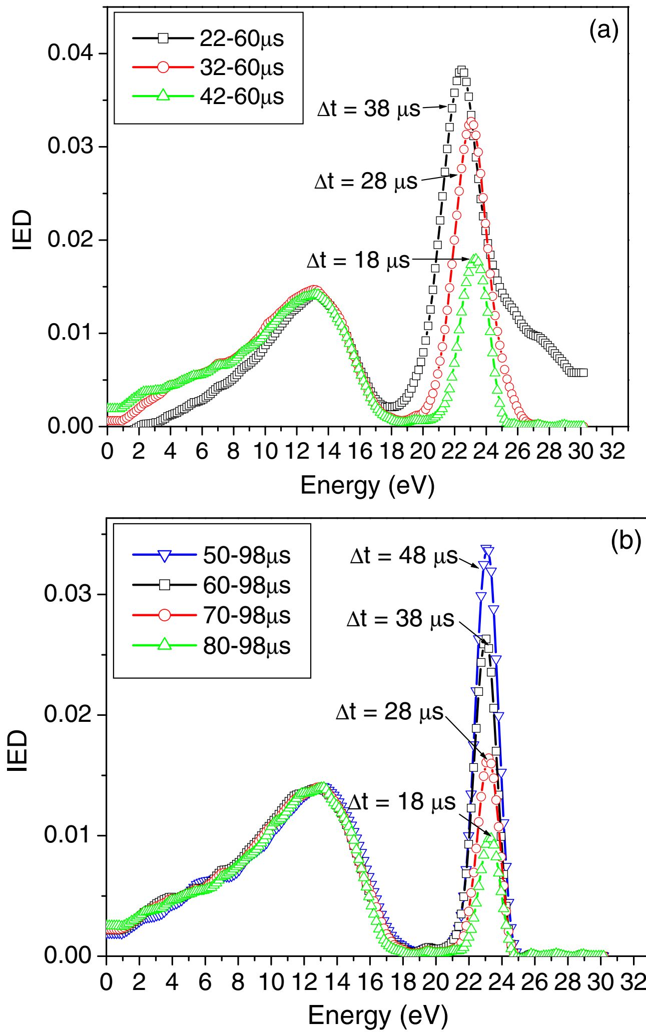

Figure 7. IEDs by applying a synchronous +24.4 V dc bias on the boundary electrode during the afterglow of a pulsed plasma for different bias starting times t_b and bias time windows, Δt_b. Other conditions: 120 W average power, 20% duty cycle, 10 kHz modulation frequency, 14 mTorr and 40 sccm. (*a*) Bias starting in the early afterglow: $t_b = 22\,\mu$s, $32\,\mu$s, and $42\,\mu$s, with $\Delta t_b = 38\,\mu$s, $28\,\mu$s, and $18\,\mu$s, respectively. (*b*) Bias starting in the late afterglow: $t_b = 50\,\mu$s, $60\,\mu$s, $70\,\mu$s and $80\,\mu$s, with $\Delta t_b = 48\,\mu$s, $38\,\mu$s, $28\,\mu$s and $18\,\mu$s, respectively.

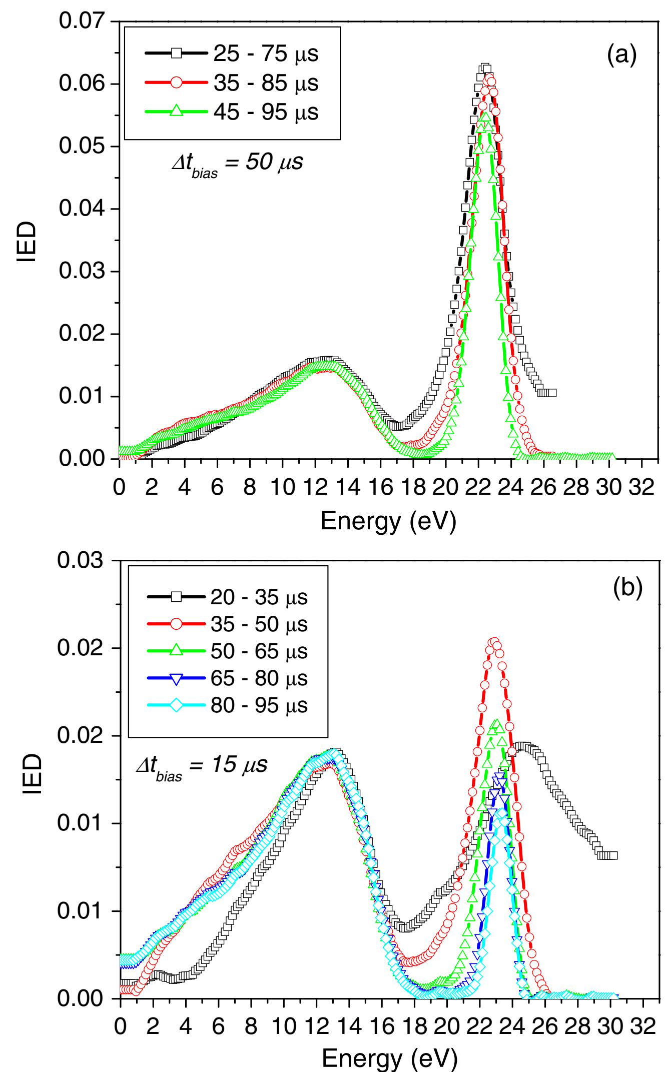

Figure 8. IEDs by applying a synchronous +24.4 V dc bias on the boundary electrode during the afterglow of a pulsed plasma for different bias starting times t_b but for the same bias time window, Δt_b. Other conditions: 120 W average power, 20% duty cycle, 10 kHz modulation frequency, 14 mTorr and 40 sccm. (*a*) $\Delta t_b = 50\,\mu s$ ($t_b = 25\,\mu s$, $35\,\mu s$, and $45\,\mu s$). (*b*) $\Delta t_b = 15\,\mu s$ ($t_b = 20\,\mu s$, $35\,\mu s$, $50\,\mu s$, $65\,\mu s$ and $80\,\mu s$).

separation between these two thresholds. The fraction of ions under each peak can also be optimized by varying the duty cycle of the pulsed plasma and/or the length of time in the afterglow during which the dc bias is applied, as discussed next.

3.2.2.2. Effect of bias timing in the afterglow. IEDs in the afterglow were also measured with a synchronous dc bias (+24.4 V) applied to the boundary electrode for different start times (t_b) and time windows (Δt_b). The pulsed plasma was generated with 120 W average power, at 10 kHz and 20% duty cycle, 14 mTorr and 40 sccm Ar flow rate. IEDs with the dc bias applied in the early afterglow and late afterglow are shown in figures 7(*a*) and (*b*), respectively. In figure 7(*a*) biasing starts at progressively later times in the afterglow and ends 60 μs into the pulse (or 40 μs into the afterglow), thus Δt_b varies from 18 to 38 μs. As in figure 6, the higher energy peaks correspond to the applied bias, whereas the lower energy peaks correspond to V_P without bias. When biasing starts at $t_b = 22\,\mu$s (only 2 μs after plasma turn OFF) T_e is still high (figure 4) resulting in a broader width of the respective high energy peak. As t_b is delayed further into the afterglow, T_e decreases and so does the width of the higher energy peaks of the IED. In figure 7(*b*) biasing starts deep into the afterglow when T_e changes little with time (figure 4). Therefore, the width of the IED is hardly affected by the biasing starting time t_b. In both figures 7(*a*) and (*b*), the collected ion current is larger as Δt_b increases.

In figure 8 t_b was varied while keeping a constant Δt_b of 50 μs or 15 μs. The average power into the pulsed plasma was 120 W. When the biasing window is long (50 μs) compared with the T_e decay time ($\sim$10 μs), the biasing starting time hardly affects the IED (figure 8(*a*)). This is because the average T_e over these bias windows are low and roughly equal. When

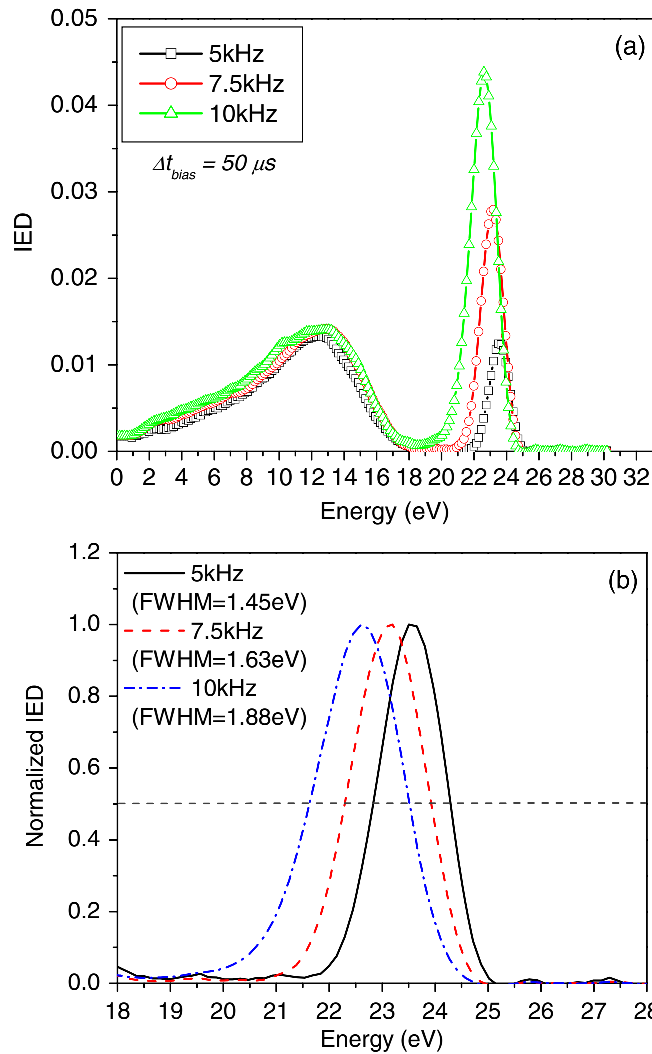

Figure 9. IEDs by applying a synchronous +24.4 V dc bias during the afterglow of a pulsed plasma for different plasma modulation frequencies. Other conditions: 120 W average power, 20% duty cycle, 14 mTorr and 40 sccm. (*a*) Bias duration $\Delta t_b = 50\,\mu$s, and bias starting times t_b are 145 μs, 75 μs, and 45 μs for modulation frequency of 5 kHz, 7.5 kHz and 10 kHz, respectively. (*b*) Normalized IEDs with FWHM of 1.45 eV, 1.63 eV and 1.88 eV, respectively, at 5 kHz, 7.5 kHz and 10 kHz.

Δt_b is short (15 μs), however, a biasing starting time in the early afterglow ($t_b = 20\,\mu$s) results in a broad IED peak (figure 8(*b*)). The width of the IED diminishes progressively, as t_b is shifted to later times in the afterglow. Again, the width of the IED correlates with T_e during the corresponding biasing window.

Further experiments were conducted varying the plasma power modulation frequency (5, 7.5 and 10 kHz) while keeping a constant $\Delta t_b = 50\,\mu$s (figure 9). The pulsed plasma was generated at 14 mTorr Ar pressure with a 20% duty cycle, and an average power of 120 W. As the modulation frequency decreases (keeping the same duty cycle), the duration of both the active glow and the afterglow increase. In this case, t_b was 145 μs, 75 μs and 45 μs for modulation frequency of 5 kHz, 7.5 kHz and 10 kHz, respectively. For all three modulation frequencies, the low energy peaks are nearly identical because of the same average power and accordingly the same V_P of

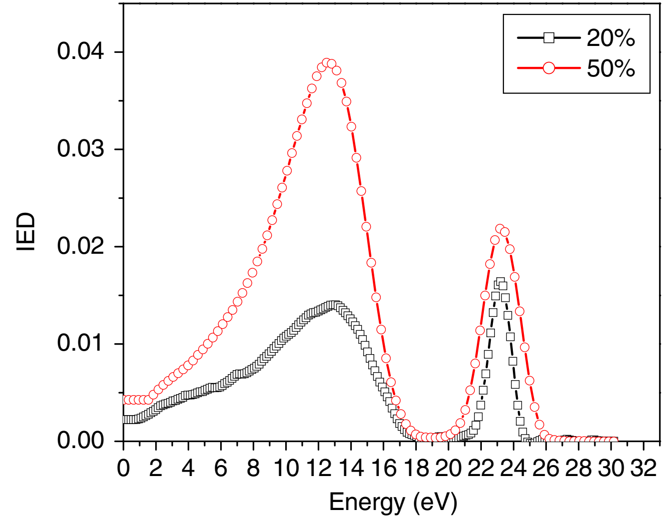

Figure 10. IEDs by applying a synchronous +24.4 V dc bias on the boundary electrode during the afterglow ($\Delta t_b = 70$ to 98 μs) of a pulsed plasma for different duty cycles. Other conditions: 10 kHz power modulation frequency, 14 mTorr and 40 sccm. The average power was 120 W and 280 W for 20% and 50% duty cycle, respectively.

the active glow under constant pressure. On the other hand, the higher energy peak becomes narrower and smaller as the modulation frequency decreases because the plasma decays for a longer period at a lower modulation frequency, resulting in a lower T_e and n_i. The narrowing of the FWHM of the peak with decreasing modulation frequency is more clearly shown by the normalized curves of figure 9(*b*).

IEDs for 14 mTorr Ar pulsed plasmas at two different duty cycles (20% and 50%) are shown in figure 10. A synchronous dc bias of +24.4 V was applied from 70 to 98 μs in the afterglow. The average power was 120 W and 280 W for 20% and 50% duty cycle, respectively at 10 kHz modulation frequency. The area under the peaks is higher for the longer duty cycle. The higher energy peak has a smaller width for 20% duty cycle since the plasma decays for longer time resulting in a lower T_e and V_P. Unlike the 20% duty cycle case, T_e is still considerably high during the application of bias for the 50% duty cycle, as shown in figure 4, resulting in a residual V_P that is as high as 3.7 V, compared with only 1.9 V for the 20% duty cycle. This difference in the residual V_P explains the different widths of the respective IEDs in figure 10.

The area under the peak of the IED is proportional to the ion charge collected during the biasing window. This charge was estimated using the Bohm flux of ions $J_o = en_s u_B$, where n_s is the ion density at the sheath edge and u_B is the Bohm velocity and the known biasing times. Using the measured ion density n_b ($n_s = 0.6n_b$) and electron temperature averaged over the duration of the bias, the estimated ion charge was indeed found to be proportional to the area under the respective peaks of figures 7–10.

3.2.3. Energy spread of the IED. The full width at half maximum (FWHM) of the peaks corresponding to the applied dc bias increases with pressure from 1.7 eV at 7 mTorr to 2.5 eV at 50 mTorr (figure 6). These peaks are much tighter than

those of the ions from the active glow with no bias, though still broader than the energy resolution of the RFEA. The latter was estimated to be $\Delta E/E \sim 2\%$, [31] or a FWHM of 0.5 eV for $E = 25$ V. Collisions in the differentially pumped RFEA can be ignored, since the local pressure was about two orders of magnitude lower than the discharge pressure, making the ion mean free path (∼15 cm corresponding to the highest plasma pressure used) much longer than the analyzer length of ∼1 cm.

Some ion–neutral collisions do occur in the sheath. These could contribute to the 'tail' of the IED to the left of the peaks at higher pressures, but are not expected to be the major cause of the observed widths of 1.7 to 2.5 eV in the afterglow. For instance, the ion mean free path at 14 mTorr is about $\lambda_i = 0.2$ cm which is a factor of 10 larger than the sheath width ($s \sim 200\,\mu$m, estimated from the Child law [1]). This results in an ion collision probability $P_c = 1 - \exp(-s/\lambda_i)$ of ∼10%. Note that the plasma density increases strongly with pressure, causing the sheath width to decrease, counteracting the decrease in mean free path with pressure. Ion–neutral collisions in the presheath can contribute significantly to the spread of the IED. Depending on the ion collisionality, the FWHM of the IED can be several T_e (see figure 4 of [33]).

Transient perturbations caused by the application and cessation of a dc bias pulse during the afterglow may also be contributing to the broadening of the IED. Figure 11 shows time-dependent LP I–V characteristics recorded during the afterglow period for two different dc biasing starting times, 30 μs (figure 11(*a*)) and 70 μs (figure 11(*b*)). Regardless of the biasing starting time, there is a ∼10 μs period during which the shape of the I–V curve transitions from one with a well defined V_P at low potential to one with a similar shape but shifted by ∼21 V, corresponding to the V_P with the dc bias ON. During the transition, the plasma seems to be undergoing a complex adjustment, which can even give rise to instabilities (note the oscillations in the current at 4–6 μs after the application of the dc bias pulse). Similar effects occur when the bias pulse extinguishes. During these periods there is rapid expansion and contraction of the sheath above the RFEA as well as transient charging and discharging of the insulating alumina tube that contains the plasma. Therefore ions crossing the sheath above the RFEA during these periods will experience transients in V_P which could contribute to the observed small amount of broadening of the IEDs.

4. Conclusions

A retarding field energy analyzer was employed to study ion energy distributions on a grounded substrate in contact with a Faraday-shielded argon inductively coupled plasma, sustained in a cylindrical discharge tube. Both cw and power modulated (pulsed) plasmas were investigated. A movable Langmuir probe was used to measure space- and time-resolved plasma parameters (electron and ion density, electron temperature, plasma potential) along the axis of the discharge tube. For a cw plasma without any bias voltage applied, the IED exhibited a single peak at V_P. The peak ion energy decreased with increasing pressure (7–50 mTorr) following the decrease in V_P. The single-peaked IED shifted to higher energies by the

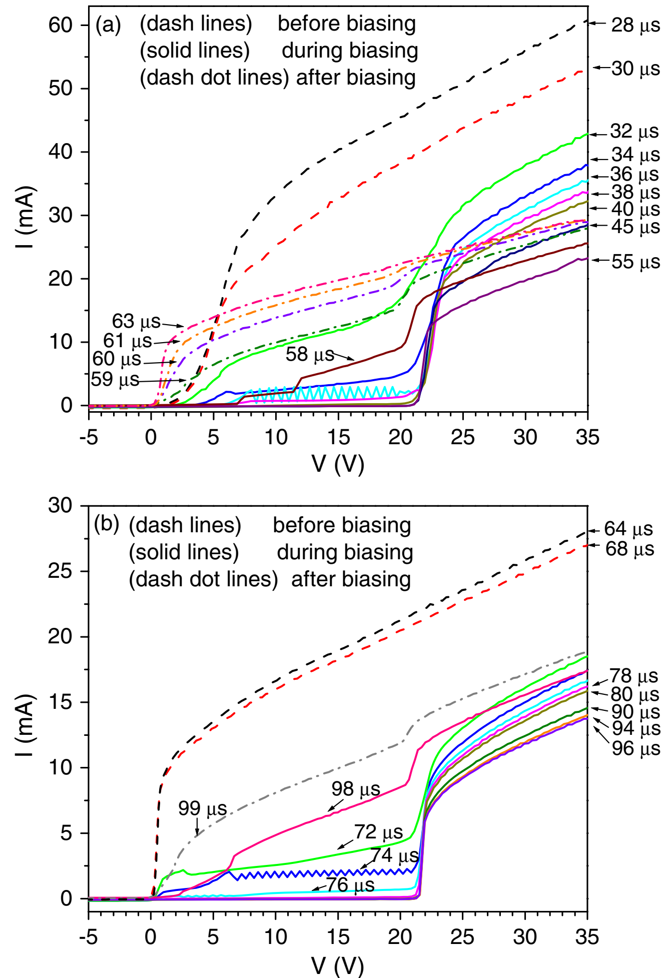

Figure 11. LP I–V curves during the afterglow of a pulsed plasma. A dc bias pulse was applied synchronously, starting at 30 μs and ending at 58 μs (*a*), or starting at 70 μs and ending at 98 μs (*b*). I–V characteristics before, during, and after dc biasing, are shown as dotted, solid, and dashed–dotted curves, respectively. Other conditions: 120 W average power, 20% duty cycle, 10 kHz modulation frequency, 14 mTorr and 40 sccm.

application of a *continuous* positive dc bias on a 'boundary electrode' in contact with the plasma. The energy shift was controlled by the value of the boundary voltage and followed the change in V_P, as measured by the LP.

The application of a dc bias on the boundary electrode under pulsed-plasma conditions resulted in a double-peaked IED. One relatively broad peak corresponded to ions bombarding the substrate during the plasma ON phase of the cycle, while the second sharper peak corresponded to the applied dc bias voltage. By employing a pulsed plasma and a (pulsed) synchronous dc bias on the boundary electrode during the afterglow, the energies of the two peaks, as well as the separation between the peaks, could be precisely controlled. This is important for practical etching processes which require very high selectivity. The full width at half maximum of the sharp peak correlated with the electron temperature during the afterglow. The FWHM could be made smaller by extending the afterglow duration (smaller duty ratio or smaller plasma power modulation frequency), applying the synchronous dc bias at later times in the afterglow, or extending the time

window in the afterglow during which dc bias was applied. All these situations were characterized by lower T_e during the application of dc bias, resulting in smaller FWHM of the respective IED. Ion–neutral collisions, especially in the presheath, and transients in the plasma potential during the application and cessation of the dc bias in the afterglow, could be contributing to the broadening of the IEDs beyond the resolution of the RFEA.

Acknowledgments

This work was supported by the Department of Energy, Office of Fusion Energy Science, contract DE-SC0001939, the National Science Foundation grant CBET 0903426, the Department of Energy grant DE-SC0000881 and VARIAN Semiconductor Associates.

References

[1] Lieberman M A and Lichtenberg A J 1994 *Principles of Plasma Discharges and Materials Processing* (New York: Wiley)
[2] Report of the Department of Energy 2008 Low temperature plasma science: not only the fourth state of matter but all of them
[3] Wang S-B and Wendt A E 2001 Ion bombardment energy and SiO_2/Si fluorocarbon plasma etch selectivity *J. Vac. Sci. Technol.* A **19** 2425
[4] Wang S-B and Wendt A E 2000 Control of ion energy distribution at substrates during plasma processing *J. Appl. Phys.* **88** 643
[5] Qin X V, Ting T-H and Wendt A E 2010 Tailored ion energy distributions at an rf-biased plasma electrode *Plasma Sources Sci. Technol.* **19** 065014
[6] Athavale S D and Economou D J 1995 Molecular dynamics simulation of atomic layer etching of silicon *J. Vac. Sci. Technol.* A **13** 966
[7] Athavale S D and Economou D J 1996 Realization of atomic layer etching of silicon *J. Vac. Sci. Technol.* B **14** 3702
[8] Panda S and Economou D J 2001 Anisotropic etching of polymer films by high energy oxygen atom neutral beams *J. Vac. Sci. Technol.* A **19** 398
[9] Kokkoris G, Tserepi A and Gofolides E 2008 The potential of neutral beams for deep silicon nanostructure etching *J. Phys. D: Appl Phys.* **41** 024004
[10] Xu L, Nasrullah A, Chen X, Jain M, Ruchhoeft P, Economou D J and Donnelly V M 2008 Etching of nanopatterns in silicon using nanopantography *Appl. Phys. Lett.* **92** 013124
[11] Xu L, Vemula S C, Jain M, Nam S K, Donnelly V M, Economou D J and Ruchhoeft P 2005 Nanopantography: a new method for massively parallel nanopatterning over large areas *Nano Lett.* **5** 2563
[12] Sobolewski M A, Olthoff J K and Wang Y 1999 Ion energy distributions and sheath voltages in a radio-frequency-biased, inductively coupled, high-density plasma reactor *J. Appl. Phys.* **85** 3966
[13] Kohler K, Horne D E and Coburn J W 1985 Frequency dependence of ion bombardment of grounded surfaces in rf argon glow discharges in a planar system *J. Appl. Phys.* **58** 3350
[14] Kuypers A D and Hopman H J 1990 Measurement of ion energy distributions at the powered rf electrode in a variable magnetic field *J. Appl. Phys.* **67** 1229
[15] Kawamura E, Vahedi V, Lieberman M A and Birdsall C K 1999 Ion energy distributions in rf sheath; review, analysis and simulation *Plasma Sources Sci. Technol.* **8** R45
[16] Woodworth J R, Abraham I C, Riley M E, Miller P A, Hamilton T W, Aragon B P, Shul R J and Willison C G 2002 Ion energy distributions at rf-biased wafer surfaces *J. Vac. Sci. Technol.* A **20** 873
[17] Gahan D, Dolinaj B and Hopkins M B 2008 Retarding field analyzer for ion energy distribution measurements at a radio-frequency biased electrode *Rev. Sci. Instrum.* **79** 033502
[18] Metze A, Ernie D W and Oskam H J 1989 The energy distribution of ions bombarding electrode surfaces in rf plasma reactors *J. Appl. Phys.* **65** 993
[19] Kortshagen U and Zethoff M 1995 Ion energy distribution functions in a planar inductively coupled RF discharge *Plasma Sources Sci. Technol.* **4** 541
[20] Stevens J E, Sowa M J and Cecchi J L 1996 Uniformity of radio frequency bias voltages along conducting surfaces in a plasma *J. Vac. Sci. Technol.* A **14** 139
[21] Smith B A and Overzet L J 1997 Ion energy control in an insulating inductively coupled discharge reactor *Appl. Phys. Lett.* **70** 1950
[22] Coburn J W and Kay E 1972 Positive-ion bombardment of substrates in rf diode glow discharge sputtering *J. Appl. Phys.* **43** 4965
[23] Xu L, Economou D J, Donnelly V M and Ruchhoeft P 2005 Extraction of a nearly monoenergetic ion beam using a pulsed plasma *Appl. Phys. Lett.* **87** 041502
[24] Malyshev M V and Donnelly V M 2000 Diagnostics of chlorine inductively coupled plasmas: measurement of electron temperatures and electron energy distribution functions *J. Appl. Phys.* **87** 1642
[25] Malyshev M V and Donnelly V M 2001 Diagnostics of inductively coupled chlorine plasmas: Measurement of electron and total positive ion densities *J. Appl. Phys.* **90** 1130
[26] Annaratone B M, Allen M W and Allen J E 1992 Ion currents to cylindrical Langmuir probes in RF plasmas *J. Phys. D: Appl. Phys.* **25** 417
[27] Rousseau A, Teboul E, Béchu S 2005 Comparison between Langmuir probe and microwave autointerferometry measurements at intermediate pressure in an argon surface wave discharge *J. Appl. Phys.* **98** 083306
[28] Malyshev M V, Donnelly V M, Colonell J I and Samukawa S 1999 Dynamics of pulsed-power chlorine plasmas *J. Appl. Phys.* **86** 4813
[29] Malyshev M V and Donnelly V M 2000 Dynamics of inductively-coupled pulsed chlorine plasmas in the presence of continuous substrate bias *Plasma Sources Sci. Technol.* **9** 353
[30] Kim C-K and Economou D J 2002 Plasma molding over surface topography: energy and angular distribution of ions extractd out of large holes *J. Appl. Phys.* **91** 2594
[31] Sakai Y and Katsumata I 1985 An energy resolution formula of a three plane grids retarding field energy analyzer *Japan. J. Appl. Phys.* **24** 337–41
[32] Riemann K-U 1981 Kinetic theory of the plasma sheath transition in a weakly ionized plasma *Phys. Fluids* **24** 2163
[33] Riemann K-U 2003 Kinetic analysis of the collisional plasma-sheath transition *J. Phys. D: Appl. Phys.* **36** 2811–20
[34] Biondi M A 1954 Diffusion cooling of electrons in ionized gases *Phys. Rev.* **93** 1136
[35] Gorchakov S, Loffhagen D and Uhrlandt D 2006 Role of excited atoms in decaying low-pressure argon plasma *Phys. Rev.* E **74** 066401
[36] Nam S K, Economou D J and Donnelly V M 2007 Particle-in-Cell simulation of ion beam extraction from a pulsed plasma through a grid *Plasma Sources Sci. Technol.* **16** 90